arXiv:1510.08650v1 [cond-mat.str-el] 29 Oct 2015

Time-dependent many-body treatment of electron-boson dynamics: application to plasmon-accompanied photoemission

M. Schüler,* J. Berakdar, and Y. Pavlyukh
Institut für Physik, Martin-Luther-Universität Halle-Wittenberg, 06099 Halle, Germany
(Dated: October 30, 2015)

Recent experiments access the time-resolved photoelectron signal originating from plasmon satellites in correlated materials and address their build-up and decay in real time. Motivated by these developments, we present the Kadanoff-Baym formalism for the nonequilibrium time evolution of interacting fermions and bosons. In contrast to the fermionic case the bosons are described by second-order differential equations. Solution of the bosonic Kadanoff-Baym equations — which is the central ingredient of this work — requires substantial modification of the usual two-times electronic propagation scheme. The solution is quite general and can be applied to a number of problems, such as the interaction of electrons with quantized photons, phonons and other bosonic excitations. Here, the formalism is applied to the photoemission from a deep core hole accompanied by plasmon excitation. We compute the time-resolved photoelectron spectra and discuss the effects of *intrinsic* and *extrinsic* electron energy losses and their interference.

I. INTRODUCTION

The impressive advances in the field of attosecond metrology[1–4] lead to new insights into the transient electron dynamics in atomic[5], molecular[6] and condensed[7] matter. The attosecond streaking technique in particular captures the *time-resolved* photoelectron spectra and thus allows for tracing the pathway of plasmon-accompanied photoemission in the time domain[8–10].

Generally, photoemission is an involved process[11] in which several factors are important: the density of states of the unperturbed system, the electron scattering following photoabsorption and the formation of electron scattering states which are subsequently observed in the detector. The corresponding three stages are known as the classical model of photoemission due to Berglund and Spicer[12]. The last stage is complicated by the presence of long-range Coulomb interaction between the emitted particle and the target. Fortunately, in many cases calculations of the scattering states can be decoupled from the treatment of the many-body effects, which is the main topic of this work.

A deep core hole is created due to the interaction with an XUV photon. The liberated electron interacts with both, the particle-hole excitations in the conduction band and may also excite collective charge density fluctuations (plasmons). The separation between these scattering mechanisms is only possible in the long wave-length limit where particle-hole excitations shape the threshold profile. The plasmons, by acting as massive bosonic particles, reshape the satellites features in the spectrum[13]. The latter effect, which is inherently nonequilibrium and known as *extrinsic* losses, should be distinguished from the *intrinsic* losses manifested as, e. g. plasmonic satellites (PSs) in the equilibrium spectral function. The occurrence of quantum interference between these two channels is essential for obtaining accurate photoemission spectra in the vicinity of PSs[14]. A microscopic theory accounting for intrinsic and extrinsic losses is a challenge even in standard steady-state photoemission theory[15–18], while a time-dependent description is still lacking.

In this work we focus on the time-dependent aspects of photoemission for electronic systems where the interaction is solely mediated by the bosonic excitations. Typical examples are processes involving electron-phonon or electron-photon interactions. Also in pure electronic systems the interaction can often be written in this form: e. g. for deep core photoemission the photoelectron at high energies can be treated as distinguishable particle interacting with the density fluctuation of the system[19]. At metallic densities fluctuations are dominated by plasmonic excitations. This gives rise to the s-model originally proposed by Lundqvist[20] and solved by Langreth[13]. Keeping in mind the distinguishability aspect of such a reduction the model can also be applied to more general scenarios such as homogeneous electron gas at metallic densities[21] or solids treated in the plasmon-pole approximation[22]. A sequence of plasmonic satellites accompanying the main quasi-particle (QP) peak is a generic feature of the density of states of the electron-boson Hamiltonian[23].

A powerful method to deal with time-dependent process in many body systems is the nonequilibrium Green function (NEGF) approach. It provides a link to standard many-body perturbation theory, allowing so for systematic approximation schemes, and also to classical kinetics[24]. On important application of the NEGF formalism is the prediction and interpretation of time-resolved angular-resolved photoemission spectra (tr-ARPES)[25] — a technique that is used in recent experiments on ultrafast dynamics of electronic[26] or phononic[27] band structures of correlated materials.

The method relies on solving the equations of motion (EOM) for the Green's functions on the Keldysh time-contour[28–30] — the Kadanoff-Baym equations (KBEs) — with a proper choice of self-energy[31–33], which in turn determines the form of collision integrals. This work is devoted to the extension of this formalism to coupled electron-boson Hamiltonians (Sec. II A) and formulation of bosonic EOM as a second order equation for massive particles (Sec. II B). The formalism is kept general and is thus applicable to related problems such as pseudo-particles[34], electron-phonon[35–39], electron-vibron[40,41] or electron-photon[42], or plasmonic nanojunctions[43,44]. In this study we go beyond the frozen boson scheme as often employed for electron-phonon coupling[45,46] and treat density oscillations in the system quan-

tum mechanically. Our time-dependent numerical approach (Sec. III) allows to disentangle intrinsic from extrinsic losses in photoemission in a natural way and complement the steady regime studies that have been performed previously[16,17,47–61].

We apply the theory to the time-resolved photoemission from the magnesium 2p core state and discuss the influence of intrinsic and extrinsic electron-plasmon couplings (Sec. IV). Atomic units are used unless stated otherwise.

II. THEORY

Our goal is the description of a system of electrons interacting with bosonic QPs that can be emitted or absorbed and thus mediate an effective electron-electron interaction. As a consequence, the boson propagators must have spectral features that are quite different from (non-relativistic) electrons: instead of one QP peak at energy $\mathcal{E}$, a boson mode with frequency Ω is represented by two peaks at $\pm\Omega$ in the spectral function $\hat{B}(\omega)$, corresponding to emission or absorption of the QP, respectively. More generally, this is reflected by the anti-symmetry of the boson spectral function $\hat{B}(\omega) = -\hat{B}^{\mathrm{T}}(-\omega)$, which make it different from that of real bosonic particles such as atoms with integer nuclear spin.

A. Generic Hamiltonian

Let us consider a system characterized by a set of electronic single-particle (SP) states with energies $\{\mathcal{E}_i\}$ and possessing a number of boson modes with corresponding frequencies $\{\Omega_\nu\}$. The respective annihilation operators of the electrons (bosons) are denoted by $\hat{c}_i$ ($\hat{a}_\nu$).

For the electrons we have the non-interacting Hamiltonian

$$\hat{H}_{\mathrm{el}} = \sum_i \mathcal{E}_i \hat{c}_i^\dagger \hat{c}_i \,, \tag{1}$$

while

$$\hat{H}_{\mathrm{bos}} = \sum_\nu \Omega_\nu \hat{a}_\nu^\dagger \hat{a}_\nu = \frac{1}{2}\sum_\nu \Omega_\nu \left(\hat{P}_\nu^2 + \hat{Q}_\nu^2\right) \tag{2}$$

represents the boson Hamiltonian. Instead of working with the bosonic creation or annihilation operators the coordinate-momentum representation,

$$\hat{Q}_\nu = \frac{1}{\sqrt{2}}\left(\hat{a}_\nu + \hat{a}_\nu^\dagger\right) \,, \quad \hat{P}_\nu = \frac{1}{\sqrt{2}\mathrm{i}}\left(\hat{a}_\nu - \hat{a}_\nu^\dagger\right) \,, \tag{3}$$

is preferred here. Note that electrons and bosons (besides their coupling) are considered as non-interacting here for the sake of a clear presentation. However, additional correlation effects for both subsystems can, in principle, be included without conceptional obstacles.

The electron-boson interaction is taken as

$$\hat{H}_{\mathrm{el-bos}} = \sum_\nu \sum_{ij} \Gamma_{ij}^\nu \hat{c}_i^\dagger \hat{c}_j \hat{Q}_\nu \,. \tag{4}$$

A coupling were the order of the fermionic operators is interchanged (e. g. $\hat{c}_i\hat{c}_j^\dagger$) can be treated along the same lines by employing the anti-commutator relation $\hat{c}_i\hat{c}_j^\dagger = \delta_{ij} - \hat{c}_j^\dagger\hat{c}_i$. The remaining term arising due to the Kronecker delta, $\sum_{\nu,i}\Gamma_{ii}^\nu\hat{Q}_\nu$ can be removed by shifting bosonic coordinates.

Furthermore we account for environmental effects such as particle exchange and line broadening by including additional baths. In analogy to above, we define the environment SP states by the energies $\{\epsilon_k\}$ whereas the boson bath is characterized by the frequencies $\{\omega_\alpha\}$.

$$\hat{H}_{\mathrm{el}}^{\mathcal{B}} = \sum_k \epsilon_k \hat{d}_k^\dagger \hat{d}_k \,, \quad \hat{H}_{\mathrm{bos}}^{\mathcal{B}} = \frac{1}{2}\sum_\alpha \omega_\alpha \left(\hat{p}_\alpha^2 + \hat{q}_\alpha^2\right) \,. \tag{5}$$

The boson bath operators $\hat{p}_\alpha$, $\hat{q}_\alpha$ are defined analogous to eq. (3), while $\hat{d}_k$ denotes the annihilation operators with respect to the electron bath. The coupling of the electron-boson system to the environmental degrees of freedom is described by the embedding Hamiltonians

$$\hat{H}_{\mathrm{el-em}} = \sum_{i,k}\left(V_{ik}\hat{c}_i^\dagger\hat{d}_k + \mathrm{h.c.}\right) \tag{6}$$

and

$$\hat{H}_{\mathrm{bos-em}} = \sum_{\alpha,\nu}\gamma_{\alpha,\nu}\hat{Q}_\nu\hat{q}_\alpha \,. \tag{7}$$

The total static Hamiltonian thus reads

$$\hat{H}_0 = \hat{H}_{\mathrm{el}} + \hat{H}_{\mathrm{bos}} + \hat{H}_{\mathrm{el-bos}} + \hat{H}_{\mathrm{el}}^{\mathcal{B}} + \hat{H}_{\mathrm{bos}}^{\mathcal{B}} + \hat{H}_{\mathrm{el-em}} + \hat{H}_{\mathrm{bos-em}} \,. \tag{8}$$

For later convenience we also introduce

$$\hat{H}_0'(t) = \hat{H}_{\mathrm{el}} + \hat{H}_{\mathrm{bos}} + s(t)\hat{H}_{\mathrm{int}} \,, \tag{9}$$

where $\hat{H}_{\mathrm{int}}$ comprises all the interacting contributions from eq. (8). The modified Hamiltonian (9) allows, by choosing a suitable functional form for the scaling factor $s(t)$, to "switch on" the interaction adiabatically in order to obtain fully correlated eigenstates of $\hat{H}_0$, while $s \equiv 1$ retrieves the static case.

To account for light-matter interaction we introduce

$$\hat{H}_{\mathrm{el-L}}(t) = \sum_{ij} F_{ij}(t)\hat{c}_i^\dagger\hat{c}_j + \mathrm{h.c.} \,, \tag{10}$$

where $F_{ij}(t)$ comprise the transition matrix elements and the time-dependent field. There is no direct coupling of light to bosonic excitations in the minimal coupling scheme. The total time-dependent Hamiltonian is then given by

$$\hat{H}(t) = \hat{H}_0'(t) + \hat{H}_{\mathrm{el-L}}(t) \,. \tag{11}$$

B. Equations of motion

To treat photoemission for the system described by the Hamiltonian (11) we proceed in a standard way by considering the one-particle fermionic and bosonic Green's functions[18,62]. Transient optical absorption requires the use of

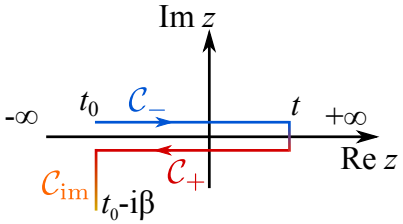

FIG. 1. The general contour C consisting of the forward branch C_- on the real axis, the backward branch C_+ and the imaginary branch $C_{\rm im}$. The arrows indicate the direction of the contour-ordering. β denotes the inverse temperature.

more complicated two-particle Green's functions[63–65] and is outside of the scope of this manuscript.

Thus, let us introduce the electron GF

$$G_{ij}(z_1,z_2) = -\mathrm{i}\langle \mathcal{T}\hat{c}_i(z_1)\hat{c}_j^\dagger(z_2)\rangle\,. \tag{12}$$

Here, z_1 and z_2 are time arguments on the general contour C[66] (sketched in fig. 1), while $\mathcal{T}$ represents the corresponding contour-ordering operator. All operators are represented in a contour Heisenberg picture. The average $\langle\dots\rangle$ refers to an initial ensemble of eigenstates of the Hamiltonian $\hat{H}^{\rm M}$. Typical choices here are (i) $\hat{H}^{\rm M} = \hat{H}_0 - \mu\hat{n}_{\rm el}$ ($\hat{n}_{\rm el}$ is the electron number operator), or (ii) $\hat{H}^{\rm M} = \hat{H}_{\rm el} + \hat{H}_{\rm bos} - \mu\hat{n}_{\rm el}$. Case (i) prepares the system in an ensemble with initial correlation, whereas in (ii) the non-interacting and thus known basis is used as reference. Adiabatic switching can then be employed to obtain a correlated state by turning on the interaction along the real time-axis[30]. Note that the chemical potential for the bosons is assumed to be zero as, in principle, an infinite number of them can be created.

Next, we define the boson GF — the coordinate-coordinate correlator — according to

$$\begin{aligned} D_{\mu\nu}(z_1,z_2) &= -\mathrm{i}[\langle \mathcal{T}\hat{Q}_\mu(z_1)\hat{Q}_\nu(z_2)\rangle - \langle\hat{Q}_\mu(z_1)\rangle\langle\hat{Q}_\nu(z_2)\rangle] \\ &= -\mathrm{i}\langle \Delta\hat{Q}_\mu(z_1)\Delta\hat{Q}_\nu(z_2)\rangle \end{aligned} \tag{13}$$

with the fluctuation operator $\Delta\hat{Q}_\nu(z) = \hat{Q}_\nu(z) - \langle\hat{Q}_\nu(z)\rangle$. Likewise the momentum-coordinate

$$D^{PQ}_{\mu\nu}(z_1,z_2) = -\mathrm{i}[\langle \mathcal{T}\hat{P}_\mu(z_1)\hat{Q}_\nu(z_2)\rangle - \langle\hat{P}_\mu(z_1)\rangle\langle\hat{Q}_\nu(z_2)\rangle]\,. \tag{14}$$

and momentum-momentum correlators

$$D^{PP}_{\mu\nu}(z_1,z_2) = -\mathrm{i}[\langle \mathcal{T}\hat{P}_\mu(z_1)\hat{P}_\nu(z_2)\rangle - \langle\hat{P}_\mu(z_1)\rangle\langle\hat{P}_\nu(z_2)\rangle]\,. \tag{15}$$

can be defined. We will demonstrate below that they are not required for the propagation of $D_{\mu\nu}(z_1,z_2)$, but are necessary if one is interested in the observables such as bosonic occupation number.

In order to elucidate the features of the respective self-energies related to the explicit time dependence, we have re-derived the EOM using the source-field method[67]. The full derivation is presented in appendix A. Here we recapitulate the key points.

The electron GF (represented as matrix) obeys, as usual,

$$\left(\mathrm{i}\frac{\partial}{\partial z_1}\mathbf{I} - \mathbf{h}^{\rm MF}(z_1)\right)\mathbf{G}(z_1,z_2) = \delta(z_1,z_2) + \int_C \mathrm{d}z_3\,\mathbf{\Sigma}(z_1,z_3)\mathbf{G}(z_3,z_2)\,. \tag{16}$$

The self-energy, comprising many-body effects due to the electron-boson interaction and the coupling to the environment, appears as a mean-field (MF) contribution incorporated into the MF Hamiltonian $\mathbf{h}^{\rm MF}$,

$$h^{\rm MF}_{ik}(z) = \mathcal{E}_i\delta_{ik} + F_{ik}(z) + s(z)\sum_\nu \Gamma^\nu_{ik}\langle\hat{Q}_\nu(z)\rangle \tag{17}$$

and as the time non-local correlation self-energy.

The EOM for the boson propagator $D_{\mu\nu}(z_1,z_2)$ can be derived (details in appendix A) from the Heisenberg EOM for position and momentum operators:

$$\frac{\mathrm{d}}{\mathrm{d}z}\hat{Q}_\nu(z) = \Omega_\nu\hat{P}_\nu(z)\,, \tag{18}$$

$$\begin{aligned} \frac{\mathrm{d}}{\mathrm{d}z}\hat{P}_\nu(z) = &-\Omega_\nu\hat{Q}_\nu(z) - s(z)\sum_{ij}\Gamma^\nu_{ij}\hat{c}_i^\dagger(z)\hat{c}_j(z) \\ &- s(z)\sum_\alpha \gamma_{\alpha,\nu}\hat{q}_\alpha(z)\,. \end{aligned} \tag{19}$$

They show that the first order equation for $D_{\mu\nu}(z_1,z_2)$ involves momentum-position correlators $D^{PQ}_{\mu\nu}$ and can only be closed as a second-order equation. The notion of the (boson) self-energy $\Pi_{\mu\nu}(z_1,z_2)$, in the same spirit as for electronic GFs, results from closing the EOM. Gathering environmental and polarization effects into $\Pi_{\mu\nu}(z_1,z_2)$, the contour EOM for the boson GF reads

$$\begin{aligned} -\frac{1}{\Omega_\nu}\left(\frac{\partial^2}{\partial z_1^2} + \Omega_\nu^2\right)D_{\mu\nu}(z_1,z_2) &= \delta_{\mu\nu}\delta(z_1,z_2) \\ &+ \sum_\xi\int_C \mathrm{d}z_3\,\Pi_{\mu\xi}(z_1,z_3)D_{\xi\nu}(z_3,z_2)\,. \end{aligned} \tag{20}$$

In contrast to the electron case (16), the boson propagators are subject to a second-order EOM.

For examining the spectral properties we define the different Keldysh components depending on which branch of the contour (fig. 1) the arguments (z_1,z_2) are located (we adopt the conventions from ref. 66). E. g. the greater/lesser boson GF $D^{\gtrless}_{\mu\nu}(t_1,t_2)$ corresponds to $D_{\mu\nu}(z_1,z_2)$ with $z_1 = t_1 \in C_\pm$ and $z_2 = t_2 \in C_\mp$. In equilibrium, $D^{\gtrless}_{\mu\nu}(t_1,t_2)$ depends on $t_1 - t_2$ only, allowing to perform the Fourier transformation $D^{\gtrless}_{\mu\nu}(\omega) = \int_{-\infty}^{\infty}\mathrm{d}t\,e^{\mathrm{i}\omega t}D^{\gtrless}_{\mu\nu}(t)$. For instance, the resulting spectral function for the non-interacting case $\Pi_{\mu\nu} = 0$ reads $b_{\mu\nu}(\omega) = \pi\delta_{\mu\nu}\,[\delta(\omega-\Omega_\nu) - \delta(\omega+\Omega_\nu)]$. The appearance of the two peaks is, as mentioned above, a consequence of the second-order EOM eq. (20). Further properties of the boson propagators are summarized in appendix B.

As detailed in appendix A, the expression for the electron self-energy due to the electron-boson interaction is given by

$$\begin{aligned} \Sigma^{\rm el-bos}_{ij}(z_1,z_2) = \mathrm{i}\,s(z_1)\sum_{\mu\nu}\sum_{nk}\sum_{ab}\Gamma^\mu_{ik}\Gamma^\nu_{ab}\int_C \mathrm{d}(z_3z_5)G_{kn}(z_1,z_3) \\ \times\Lambda_{njab}(z_3,z_2;z_5)D_{\mu\nu}(z_5,z_1^+)s(z_5)\,, \end{aligned} \tag{21}$$

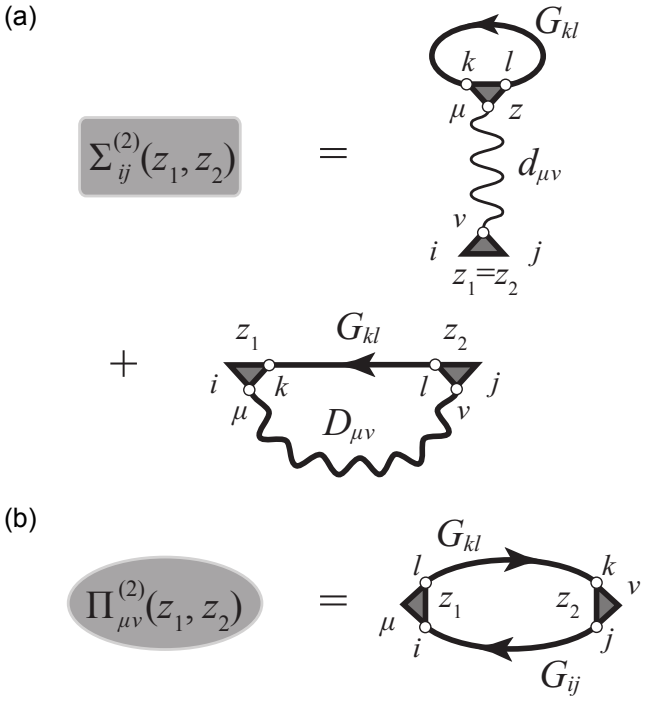

FIG. 2. Approximations for the fermionic (a) and bosonic (b) self-energy operators employed in this work. All self-energies are of the second order in $\mathbf{\Gamma}^\mu$ and are expressed in terms of full electronic $\mathbf{G}$ and bare $d_{\mu\nu}$ and full $D_{\mu\nu}$ boson propagators. The first term in the fermionic self-energy is local in time and therefore is included (see Eq. (17)) in mean-field Hamiltonian $\mathbf{h}^{\mathrm{MF}}$.

where Λ_{njab} denotes the three-point vertex function obeying the standard Bethe-Salpeter equation (BSE) with the four-point kernel $K_{abcd}(z_1,z_2;z_3,z_4) = \delta\Sigma^{\mathrm{el-bos}}(z_1,z_2)/\delta G_{cd}(z_3,z_4)$ obtained from the functional derivative of the self-energy with respect to the electron GF (details in appendix A). The boson self-energy in turn is determined by the electron (irreducible) polarization,

$$P_{abcd}(z_1,z_2) = -\mathrm{i}\sum_{pq}\int_C \mathrm{d}(z_3z_4) G_{ap}(z_1,z_3)G_{qb}(z_4,z_1^+) \times \Lambda_{pqcd}(z_3,z_4;z_2)\,, \tag{22}$$

by

$$\Pi^{\mathrm{p}}_{\mu\nu}(z_1,z_2) = s(z_1)s(z_2)\sum_{abcd}\Gamma^\mu_{ba}P_{abcd}(z_1,z_2)\Gamma^\nu_{cd}\,. \tag{23}$$

The simplest possible conserving approximation[68] emerges from invoking the zeroth-order approximation to the vertex function, that is

$$\Lambda_{abcd}(z_1,z_2;z_3) = \delta_{ac}\delta_{bd}\delta(z_1,z_2)\delta(z_1,z_3)\,. \tag{24}$$

Analogously to Hedin's equations for electronic systems (fig. 2), we designate the resulting second-order (in $\mathbf{\Gamma}$) approximations to both the electron and the boson self-energy as *GW* approximation:

$$\mathbf{\Sigma}^{(2)}(z_1,z_2) = \mathrm{i}\, s(z_1)s(z_2)\sum_{\mu\nu}\mathbf{\Gamma}^\mu\mathbf{G}(z_1,z_2)\mathbf{\Gamma}^\nu D_{\mu\nu}(z_1,z_2)\,, \tag{25a}$$

$$\Pi^{(2)}_{\mu\nu}(z_1,z_2) = -\mathrm{i}\, s(z_1)s(z_2)\mathrm{Tr}\left[\mathbf{\Gamma}^\mu\mathbf{G}(z_1,z_2)\mathbf{\Gamma}^\nu\mathbf{G}(z_2,z_1)\right]\,. \tag{25b}$$

The contribution to the respective self-energies arising from the environmental coupling (embedding self-energies) are expressed in the standard way in terms of the bath propagators for electrons:

$$\Sigma^{\mathrm{em}}_{ij}(z_1,z_2) = s(z_1)s(z_2)\sum_k V_{ik}V^*_{kj}g^{\mathcal{B}}_k(z_1,z_2)\,, \tag{26}$$

and for bosons

$$\Pi^{\mathrm{em}}_{\nu}(z_1,z_2) = s(z_1)s(z_2)\sum_\alpha \left|\gamma_{\alpha,\nu}\right|^2 d^{\mathcal{B}}_\alpha(z_1,z_2)\,. \tag{27}$$

Here, $g^{\mathcal{B}}_k$ and $d^{\mathcal{B}}_\alpha$ are the bare GFs of the respective baths. It should be noted that here the boson embedding self-energy is labeled by a single mode index ν. In general, non-diagonal terms can occur due to indirect coupling via the bath. Thus, eq. (27) relies on the assumption that such effects can be neglected. As usual, the full self-energy is obtained by summing the system and the bath contributions, that is $\mathbf{\Sigma} = \mathbf{\Sigma}^{\mathrm{el-bos}} + \mathbf{\Sigma}^{\mathrm{em}}$ and $\Pi_{\mu\nu} = \Pi^{\mathrm{p}}_{\mu\nu} + \Pi^{\mathrm{em}}_{\mu\nu}$, respectively.

Eq. (20) for the coordinate-coordinate correlator $D_{\mu\nu}(z_1,z_2)$ is not sufficient to fully describe the boson dynamics, as the MF Hamiltonian (17) explicitly depends on $\langle\hat{Q}_\nu(z)\rangle$ (this quantity can not be inferred from $D_{\mu\nu}(z_1,z_2)$). An additional EOM is therefore required and can be derived from eq. (18) and (19). Eliminating the bath amplitudes $\hat{q}_\alpha(z)$ by the standard embedding technique, one obtains

$$-\frac{1}{\Omega_\nu}\left(\frac{\partial^2}{\partial z^2}+\Omega_\nu^2\right)\langle\hat{Q}_\nu(z)\rangle = -\mathrm{i}\,\mathrm{Tr}\left[\mathbf{\Gamma}^\nu\mathbf{G}(z,z^+)\right] + \int_C \mathrm{d}\bar{z}\,\Pi^{\mathrm{em}}_\nu(z,\bar{z})\langle\hat{Q}_\nu(\bar{z})\rangle \tag{28}$$

The EOM (16), (20), (28) for quantities on the contour is to be solved together with Kubo-Martin-Schwinger (KMS) boundary conditions[69]. For eq. (28) this implies that the solution is separated into a boundary-value problem for $z = -\mathrm{i}\tau \in C_{\mathrm{im}}$, as $\langle\hat{Q}_\nu(0)\rangle = \langle\hat{Q}_\nu(-\mathrm{i}\beta)\rangle$, whereas for $z \in C_\pm$ eq. (28) represents an initial-value problem.

In absence of environmental coupling (i. e. $\Pi^{\mathrm{em}}_\nu = 0$), eq. (28) can be solved in terms of the non-interacting boson propagators $d_\nu(z_1,z_2)$, yielding

$$\langle\hat{Q}_\nu(z)\rangle = -\mathrm{i}\int_C \mathrm{d}\bar{z}\, d_\nu(z,\bar{z})\mathrm{Tr}\left[\mathbf{\Gamma}^\nu\mathbf{G}(\bar{z},\bar{z}^+)\right]\,. \tag{29}$$

Substituting eq. (29) back into the MF Hamiltonian (17) we obtain the first diagram depicted in fig. 2(a). Thus, the first-order (in $\mathbf{\Gamma}^\nu$) MF expression has been transformed to a (formally) second-order self-energy, which is often referred to as Hartree term[37,70]. We stress that this transition is not possible in presence of a boson bath ($\Pi^{\mathrm{em}}_\nu \neq 0$). The MF part will hence be kept in the more general form eq. (17). This is analogous to ref. 71.

Furthermore, propagating the boson amplitude $\langle\hat{Q}_\nu(z)\rangle$ is

necessary for computing the boson occupation number N_ν:

$$\begin{aligned} N_\nu(z) &= \langle \hat{a}_\nu^\dagger(z)\hat{a}_\nu(z)\rangle = \frac{1}{2}\left[\langle \hat{P}_\nu(z)^2\rangle + \langle \hat{Q}_\nu(z)^2\rangle - 1\right] \\ &= \frac{\mathrm{i}}{2}\left[D_{\nu\nu}(z,z^+) + D^{PP}_{\nu\nu}(z,z^+)\right] \\ &\quad + \frac{1}{2}\left[\langle \hat{P}_\nu(z)\rangle^2 + \langle \hat{Q}_\nu(z)\rangle^2 - 1\right] . \end{aligned} \tag{30}$$

III. NUMERICAL IMPLEMENTATION

In this section we revisit the formulation of the KBE from the contour EOM. Since the general solution strategy in case of electron GFs is quite established[28–30], we keep the discussion brief and rather focus on the modifications to be made for calculating the bosonic time-evolution.

Together with the corresponding adjoint EOM, eq. (16) and (20) represent the KBEs for the coupled electron-boson system that needs to be solved along with eq. (28). For a numerical approach, the general complex contour arguments are mapped onto observable times by splitting the general GFs into their respective Keldysh components. Let us introduce the convolution operations

$$[f\cdot g](t,t') \equiv \int_{t_0}^{\infty} \mathrm{d}\bar{t}\, f(t,\bar{t})g(\bar{t},t') , \tag{31}$$

$$[f\star g](t,t') \equiv -\mathrm{i}\int_0^{\beta} \mathrm{d}\bar{\tau}\, f(t,\bar{\tau})g(\bar{\tau},t') . \tag{32}$$

Applying the Langreth rules[66], the KBEs for the greater/lesser electron GF becomes

$$\mathrm{i}\frac{\partial}{\partial t_1}\mathbf{G}^{\gtrless}(t_1,t_2) = \mathbf{h}^{\mathrm{MF}}(t_1)\mathbf{G}^{\gtrless}(t_1,t_2) + \mathbf{X}_L^{\gtrless}(t_1,t_2) , \tag{33a}$$

$$-\mathrm{i}\frac{\partial}{\partial t_2}\mathbf{G}^{\gtrless}(t_1,t_2) = \mathbf{G}^{\gtrless}(t_1,t_2)\mathbf{h}^{\mathrm{MF}}(t_2) + \mathbf{X}_R^{\gtrless}(t_1,t_2) , \tag{33b}$$

$$\mathrm{i}\frac{\partial}{\partial t}\mathbf{G}^{\rceil}(t,\tau) = \mathbf{h}^{\mathrm{MF}}(t)\mathbf{G}^{\rceil}(t,\tau) + \mathbf{X}_L^{\rceil}(t,\tau) , \tag{33c}$$

with the standard collision integrals

$$\mathbf{X}_L^{\gtrless}(t_1,t_2) = \left[\mathbf{\Sigma}^{\mathrm{R}}\cdot\mathbf{G}^{\gtrless} + \mathbf{\Sigma}^{\gtrless}\cdot\mathbf{G}^{\mathrm{A}} + \mathbf{\Sigma}^{\rceil}\star\mathbf{G}^{\lceil}\right](t_1,t_2) , \tag{34a}$$

$$\mathbf{X}_R^{\gtrless}(t_1,t_2) = \left[\mathbf{G}^{\mathrm{R}}\cdot\mathbf{\Sigma}^{\gtrless} + \mathbf{G}^{\gtrless}\cdot\mathbf{\Sigma}^{\mathrm{A}} + \mathbf{G}^{\rceil}\star\mathbf{\Sigma}^{\lceil}\right](t_1,t_2) , \tag{34b}$$

$$\mathbf{X}_L^{\rceil}(t,\tau) = \left[\mathbf{\Sigma}^{\mathrm{R}}\cdot\mathbf{G}^{\rceil} + \mathbf{\Sigma}^{\rceil}\star\mathbf{G}^{\mathrm{M}}\right](t,\tau) . \tag{34c}$$

Similarly to eq. (33) one finds the KBEs for the boson propagators,

$$-\frac{1}{\Omega_\mu}\left(\frac{\partial^2}{\partial t_1^2}+\Omega_\mu^2\right)D^{\gtrless}_{\mu\nu}(t_1,t_2) = Y^{\gtrless}_{L,\mu\nu}(t_1,t_2) , \tag{35a}$$

$$-\frac{1}{\Omega_\nu}\left(\frac{\partial^2}{\partial t_2^2}+\Omega_\nu^2\right)D^{\gtrless}_{\mu\nu}(t_1,t_2) = Y^{\gtrless}_{R,\mu\nu}(t_1,t_2) , \tag{35b}$$

$$-\frac{1}{\Omega_\mu}\left(\frac{\partial^2}{\partial t^2}+\Omega_\mu^2\right)D^{\rceil}_{\mu\nu}(t,\tau) = Y^{\rceil}_{L,\mu\nu}(t,\tau) , \tag{35c}$$

where the collision integrals are obtained by applying the Langreth rules analogously as in eq. (34). The symmetry properties of the GFs (and of the respective self-energies) lead to similar relations for the collision integrals:

$$\mathbf{X}_L^{\gtrless}(t_1,t_2) = -\left[\mathbf{X}_R^{\gtrless}(t_2,t_1)\right]^\dagger , \quad Y^{\gtrless}_{L,\mu\nu}(t_1,t_2) = -\left[Y^{\gtrless}_{R,\nu\mu}(t_2,t_1)\right]^* .$$

Let us now assume that the Matsubara GF for both electrons ($\mathbf{G}^{\mathrm{M}}(\tau)$) and bosons ($D^{\mathrm{M}}_{\mu\nu}(\tau)$) has been determined by solving the respective Matsubara Dyson equation. Note that the solution has to be carried out self-consistently with the EOM for the boson amplitude (eq. (28)). From the KMS conditions one finds

$$\begin{aligned} \frac{1}{\Omega_\nu}\left(\frac{\mathrm{d}^2}{\mathrm{d}\tau^2}-\Omega_\nu^2\right)Q_\nu^{\mathrm{M}}(\tau) &= -\mathrm{i}\,\mathrm{Tr}\left[\mathbf{\Gamma}^\nu\mathbf{G}^{\mathrm{M}}(0)\right] \\ &\quad + \left[\Pi_\nu^{\mathrm{em,M}}\star Q_\nu^{\mathrm{M}}\right](\tau) . \end{aligned} \tag{36}$$

Here, $Q_\nu^{\mathrm{M}}(\tau) = \langle\hat{Q}_\nu(t_0-\mathrm{i}\tau)\rangle$. Solving the imaginary track C_{im} is straightforward if one discards initial correlations, as done in the adiabatic switching method. Once the GFs at t_0 have been initialized from the Matsubara components, eq. (33) and (35) can be propagated for real times together with the boson amplitude

$$\begin{aligned} -\frac{1}{\Omega_\nu}\left(\frac{\mathrm{d}^2}{\mathrm{d}t^2}+\Omega_\nu^2\right)\langle\hat{Q}_\nu(t)\rangle &= -\mathrm{i}\,\mathrm{Tr}\left[\mathbf{\Gamma}^\nu\mathbf{G}^<(t,t)\right] \\ &\quad + \left[\Pi_\nu^{\mathrm{em,R}}\cdot\langle\hat{Q}_\nu\rangle\right](t) . \end{aligned} \tag{37}$$

The KBEs (33) for the electrons can be solved by standard techniques. Specifically, we implemented a predictor-corrector Heun method similar to ref. 72. Eq. (33a) is used for propagating $\mathbf{G}^>(t_1,t_2)$ for $t_1 > t_2$, while $\mathbf{G}^<(t_1,t_2)$ is obtained from eq. (33b) for $t_1 < t_2$ (see fig. 3(a)). Eqs. (33) are combined at $t_1 = t_2 = t$ into the time-diagonal EOM

$$\mathrm{i}\frac{\mathrm{d}}{\mathrm{d}t}\mathbf{G}^<(t,t) = \left[\mathbf{h}^{\mathrm{MF}}(t),\mathbf{G}^<(t,t)\right] + \left(\mathbf{X}_L^<(t,t)+\mathrm{h.c.}\right) . \tag{38}$$

For propagating the bosonic KBEs (35) we have chosen the Numerov method, as it provides a fourth-order scheme with minimal number of function evaluations for this specific type of differential equations. Generally, the method applies to

$$\left(\frac{\mathrm{d}^2}{\mathrm{d}t^2}+W(t)\right)F(t) = S(t) , \tag{39}$$

which is transformed (after equidistant discretization $t_{n+1}-t_n=\Delta t$) into the recursive relation

$$\widetilde{F}_{n+1} - U_n\widetilde{F}_n + \widetilde{F}_{n-1} = \frac{\Delta t^2}{12}\left(S_{n+1}+10S_n+S_{n-1}\right) . \tag{40}$$

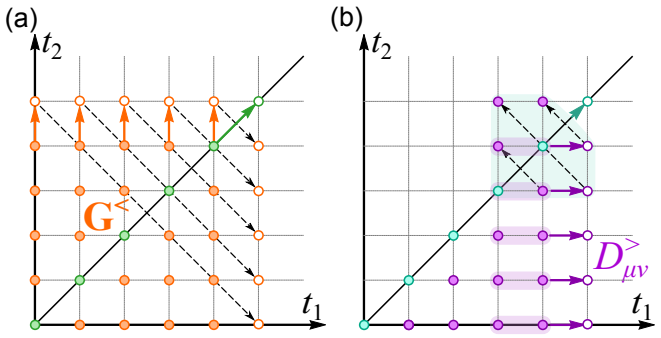

FIG. 3. Propagation scheme for solving the KBEs eq. (33) and (35). The time coordinates are discretized into a uniform mesh $\{t_n\}$, such that discrete-difference approximations can be applied to the derivatives. (a) Solution scheme for the electron KBEs. $\mathbf{G}^<(t_k, t_{n+1})$ is computed from (33b) (orange arrows). Analogously, $\mathbf{G}^>(t_n, t_k)$ is obtained from eq. (33a) in the lower part of the time plane. Eq. (38) is used for propagating on the time diagonal (green arrows). (b) Propagation method for the boson KBEs: $D^>_{\mu\nu}(t_{n+1}, t_k)$, $k \leq n$, is determined from $D^>_{\mu\nu}(t_{n-1}, t_k)$ and $D^>_{\mu\nu}(t_n, t_k)$, while the diagonal points are obtained from the surrounding grid points by a partial differential equation (see text). Symmetry relations between of greater/lesser components are denoted by dashed arrows.

Here, $S_n = S(t_n)$, $\widetilde{F}_n = (1-T_n)F(t_n)$, $U_n = (2+10T_n)/(1-T_n)$ and $T_n = -(\Delta t^2/12)W(t_n)$. When applying the Numerov method to the KBEs (35), $S(t)$ plays the role of the collision integral. From eq. (40) we see that $S(t_{n+1})$ required to perform the step $t_n \to t_{n+1}$ is unknown at this point (similar to the Heun propagation scheme). However, as $S(t_n)$ carries the dominant weight, we can substitute $(S_{n+1} + 10S_n + S_{n-1}) \approx 12S_n$ when executing $t_n \to t_{n+1}$ for the first time. The precision of eq. (40) is thereby reduced from fourth to second order. Once the boson propagators are known up to $t_1, t_2 \leq t_{n+1}$, the new collision integrals can be computed and the time step $t_n \to t_{n+1}$ can be carried out in fourth order according to eq. (40). The analogous strategy applies to eq. (37). We combine this corrector step with the one needed for propagating the electron GF (as the electron (boson) self-energy depends on the boson (electron) GF) and iterate until self-consistency at each time step is achieved.

There is no need for computing $D^<_{\mu\nu}(t_1, t_2)$ for $t_1 < t_2$ from eq. (35b), as $D^<_{\mu\nu}(t_1, t_2) = D^>_{\nu\mu}(t_2, t_1) = -[D^>_{\mu\nu}(t_1, t_2)]^*$ (cf. appendix B). Therefore, the propagation scheme can be restricted to the lower time half-plane $t_2 \leq t_1$ for the greater bosonic correlator (see fig. 3(b)). At variance with the electron KBEs it is not possible to formulate the time-diagonal EOM in the form of eq. (38), as it relies on the notion of first derivatives. We solve this issue by adding eq. (35a) and (35b) to obtain the Poisson-type equation

$$-\frac{1}{\Omega_\mu + \Omega_\nu}\left(\frac{\partial^2}{\partial t_1^2} + \frac{\partial^2}{\partial t_2^2} + \Omega_\mu^2 + \Omega_\nu^2\right) D^>_{\mu\nu}(t_1, t_2) = Z^>_{\mu\nu}(t_1, t_2)\,, \tag{41}$$

$$(\Omega_\mu + \Omega_\nu) Z^>_{\mu\nu}(t_1, t_2) = \Omega_\mu Y^>_{L,\mu\nu}(t_1, t_2) + \Omega_\nu Y^>_{R,\mu\nu}(t_1, t_2)\,. \tag{42}$$

Next we apply the two-dimensional extension of the Numerov method (see appendix C), expressing the Laplacian $\nabla^2_{t_1,t_2} D^>_{\mu\nu}(t_n, t_n)$ by the nine surrounding grid points $D^>_{\mu\nu}(t_{n+i}, t_{n+j})$, $i, j = -1, 0, 1$. The resulting equation can then be solved for $D^>_{\mu\nu}(t_{n+1}, t_{n+1})$ (sketched in fig. 3(b)). Similar to the one-dimensional case, the right-hand side of eq. (41) has to be known at all these time points, as well, in order to achieve fourth order. Analogously, we can approximate $Z^>_{\mu\nu}(t_{n+i}, t_{n+j})$ $(i, j = -1, 0, 1)$ by $Z^>_{\mu\nu}(t_n, t_n)$ when carrying out $D^>_{\mu\nu}(t_n, t_n) \to D^>_{\mu\nu}(t_{n+1}, t_{n+1})$ for the first time (predictor step) and apply several corrector steps after computing $Z^>_{\mu\nu}(t_{n+1}, t_{n+1})$.

Collision integrals are computed by either Durand's rule (even number of grid points) or Simpson's rule (odd number of points). The momentum-momentum correlator required for calculating the boson occupation eq. (30) is obtained from the mixed derivative $\Omega_\mu \Omega_\nu D^{PP,>}_{\mu\nu}(t, t') = \left[\partial_t \partial_{t'} D^>_{\mu\nu}(t, t')\right]_{t=t'}$.

IV. APPLICATION TO PHOTOEMISSION FROM MAGNESIUM 2p CORE STATE

In order to illustrate our propagation method for coupled electron-boson Hamiltonians and, furthermore, explore the physics of such systems in the time domain, we apply the theory developed in sec. II to a typical process described by the s-model: the photoemission from deep core state.

In particular we consider bulk Mg, a system where recent attosecond streaking experiments[9] were able to measure the time delay of photoemission between to the 2p core state and the corresponding plasmonic satellite. The system is modeled by the Hamiltonian (11) with the static part eq. (8). We account for the 2p state, $\mathcal{E}_{i=2p}$ and two virtual states $\mathcal{E}_{i=k_{1,2}}$ representing photoelectrons. We consider one boson mode (bulk plasmon) with energy $\Omega_{pl} \simeq 10$ eV (subscript ν is dropped). For the electron-plasmon interaction (4) we distinguish intrinsic (Γ_{in}) and extrinsic ($\mathbf{\Gamma}_{ex}$) mechanisms:

$$\hat{H}_{el-pl} = \Gamma_{in} \hat{c}_{2p} \hat{c}^\dagger_{2p} \hat{Q} + \sum_{i,j \neq 2p} (\mathbf{\Gamma}_{ex})_{ij}\, \hat{c}^\dagger_i \hat{c}_j \hat{Q}\,. \tag{43}$$

The latter accommodate post-emission effects, that is inelastic scattering of the emerging photoelectron from the electron sea upon converting a part of their energy into a plasmon.

The s-model describes two phenomena: upon x-ray absorption, an excited core electron looses a part of its energy and excites a plasmon. This process is manifested as a sequence of PSs in the spectral function occurring at lower energies. For fixed detector energy, larger photon energy is needed to produce a photoelectron from PS as compared to QP. In the reciprocal process the core hole is filled upon emitting an x-ray photon. This process can be again accompanied by creating plasmons, such that the electron looses a part of its energy and emits a photon with smaller energy when recombining. For brevity we denote PSs at lower (higher) energies as PS^- (PS^+). Furthermore, the position of the QP peak $\mathcal{E}_{QP}$ is shifted by $\Gamma^2_{in}/2\Omega_{pl}$ (correlation shift)[73] to larger energy with respect to the non-interacting value $\mathcal{E}_{2p}$ when the core state is occupied, whereas $\mathcal{E}_{QP} = \mathcal{E}_{2p} - \Gamma^2_{in}/2\Omega_{pl}$ for the empty core state. The spectral functions for the two scenarios are shown in fig. 4(a).

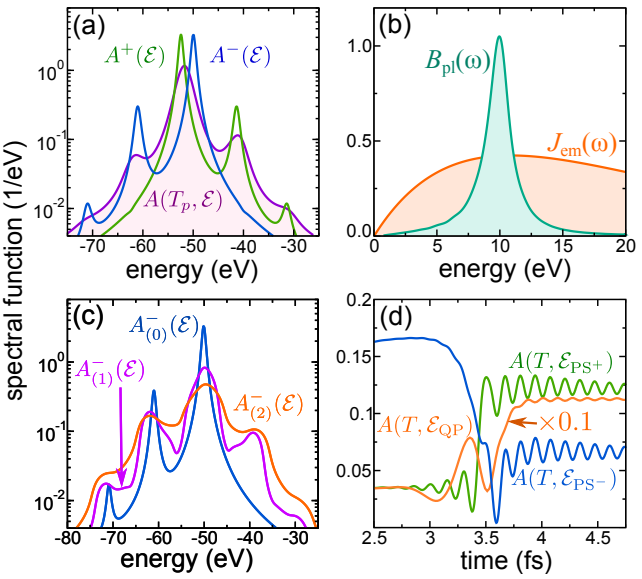

FIG. 4. (a) Spectral function $A^-(\mathcal{E})$ ($A^+(\mathcal{E})$) of occupied (empty) core state, obtained by time propagation, along with $A(T_p,\mathcal{E})$. (b) Interacting plasmon spectral function $B_{\rm pl}(\omega)$ and, for comparison, the embedding density $J_{\rm em}(\omega)$. (c) Electron spectral function $A^-_{(n)}(\mathcal{E})$ (occupied core state) with fixed plasmon occupation $N_{\rm pl} = 0, 1, 2$. (d) Dynamics of $A(T,\mathcal{E})$ for energy at the PSs and QP peak after the excitation, $\mathcal{E} = \mathcal{E}_{\rm PS^+} = -41.23$ eV, $\mathcal{E} = \mathcal{E}_{\rm PS^-} = -61.44$ eV, and $\mathcal{E} = \mathcal{E}_{\rm QP} = -51.76$ eV.

A. Time-dependent spectral function

It is now interesting to investigate the time-evolution in an intermediate case, where the initially occupied 2p state is partially photoionized, in real time. The spectral function is expected to reorganize transiently, showing i) a shift of the QP peak and ii) appearance of plasmonic satellites ($\rm PS^+$). The energetic position of these features in the spectral function varies in time primarily reflecting changes in the core state occupation and in the number of bosons in the system.

We solved the KBEs eq. (33) and (35) with the algorithm from sec. III. Instead of initializing with the interacting Matsubara GFs, we switch on the interaction adiabatically by defining $s(t) = (1 + \exp[\alpha(t_{\rm sw} - t)])^{-1}$ ($s(z) = 0$ for $z \in \mathcal{C}_{\rm im}$). Hence, initial correlations can be disregarded ($\mathbf{\Sigma}^{\rceil,\lceil} = 0$, $\Pi^{\rceil,\lceil}_{\mu\nu} = 0$), simplifying the propagation scheme. We only consider intrinsic losses in this subsection, so $\mathbf{\Gamma}_{\rm ex} = 0$.

Plasmons typically decay by exciting particle-hole (p-h) pairs (Landau damping). Beside the states already incorporated in our model, there might be other electronic transitions limiting the plasmon lifetime. p-h excitations in the conduction band in case of metals are a typical mechanism. In order to account for this plasmon decay channel in a simple way, we add a bosonic bath. For the latter we assume that the bath boson occupation number is zero, such that we obtain

$$\Pi^{\rm em,\gtrless}(t_1,t_2) = \sum_\alpha |\gamma_\alpha|^2 d^{\mathcal{B},\gtrless}_\alpha(t_1,t_2) = -\frac{\rm i}{2}\sum_\alpha |\gamma_\alpha|^2 e^{\mp {\rm i}\omega_\alpha(t_1-t_2)} \equiv -\frac{\rm i}{2}\int_0^\infty {\rm d}\omega\, J_{\rm em}(\omega) e^{\mp {\rm i}\omega(t_1-t_2)}\,, \tag{44}$$

where $J_{\rm em}(\omega)$ denotes the spectral density of the bath (it includes the coupling). For a simple Ohmic bath[74] adopted here eq. (44) can be analytically integrated:

$$J_{\rm em}(\omega) = g_0 \frac{\omega}{\omega_{\rm c}^2} e^{-\omega/\omega_{\rm c}}\,,\ \Pi^{\rm em,\gtrless}(t_1,t_2) = \frac{{\rm i}g_0}{2(\omega_c(t_1-t_2) \mp {\rm i})^2} \tag{45}$$

The transition $\omega_{\rm c} \to \infty$ represents the counterpart to the wide-band limit approximation (WBLA) often encountered for the electron embedding self-energy, as $\Pi^{\rm em,R}(t_1,t_2) \to -\pi(g_0/2\omega_{\rm c}^2)\delta'(t)$, turning the EOM (37) for the boson amplitude into the equation for the ordinary damped driven oscillator (similarly for the boson KBEs (35)), which has no memory. Adiabatic switching is realized by $g_0 \to g_0 s(t_1)s(t_2)$.

We propagated the KBEs up to $T_p = 15$ fs (time step $\Delta t = 0.024$ fs) with a switch-on time $t_{\rm sw} = 5$ fs and $\alpha = 0.1$. The inverse temperature is set to $\beta = 50$ a.u., simulating the zero-temperature case. Initially, electronic levels are occupied according to the Fermi function with chemical potential $\mu = 0$, while we assume for the plasmon occupation $N_{\rm pl}(t=0) = 0$. The environmental coupling leads to a non-zero steady-state boson number as a result of the broadening of the spectral function. For $g_0 = 1$ eV and $\omega_{\rm c} = 10$ eV we find $N_{\rm pl} = 0.012$ for $t > t_{\rm sw}$. This is in accordance with the thermodynamical equilibrium value obtained from solving the Matsubara Dyson equation for the plasmon mode (including embedding only). The boson spectral function, calculated analogously to eq. (46), is shown together with the Ohmic spectral density of the bath in fig. 4(b).

To simulate the ultra-fast photoionization dynamics, a laser pulse of 0.5 fs length and frequency $\omega_{\rm L} = 55$ eV (see fig. 5, top panel) is applied after the system is fully thermalized. For this quasi-resonant transition, we include one continuum state $|k\rangle$ at $\mathcal{E}_k = \mathcal{E}_{\rm QP} + \omega_{\rm L}$, where $\mathcal{E}_{\rm QP} = -50$ eV is the QP energy for the no-hole ground state. The light-matter interaction is simplified to $F_{2{\rm p},k}(t) = F_{k,2{\rm p}}(t) \equiv F(t)$. Electron-plasmon coupling is set to $\Gamma_{\rm in} = 5$ eV. We employ the self-energy eq. (25).

Once the solution of the KBEs has been obtained, the time-resolved spectral function can be computed by

$$\mathbf{A}(T,\mathcal{E}) = {\rm i}\int {\rm d}t\, e^{{\rm i}\mathcal{E}t}\Big[\mathbf{G}^>\Big(T+\frac{t}{2},T-\frac{t}{2}\Big) - \mathbf{G}^<\Big(T+\frac{t}{2},T-\frac{t}{2}\Big)\Big]\,. \tag{46}$$

The laser-induced dynamics is presented in fig. 5. The laser pulse (fig. 5, top panel) partially ionizes the core state (the amplitude of $F(t)$ has been chosen to maximize the depopulation) upon inducing plasmonic dynamics (fig. 5, middle panel). The creation of the core hole is faster than the plasmon time scale $\tau_{\rm pl} = 2\pi/\Omega_{\rm pl}$, indicating a strongly non-adiabatic

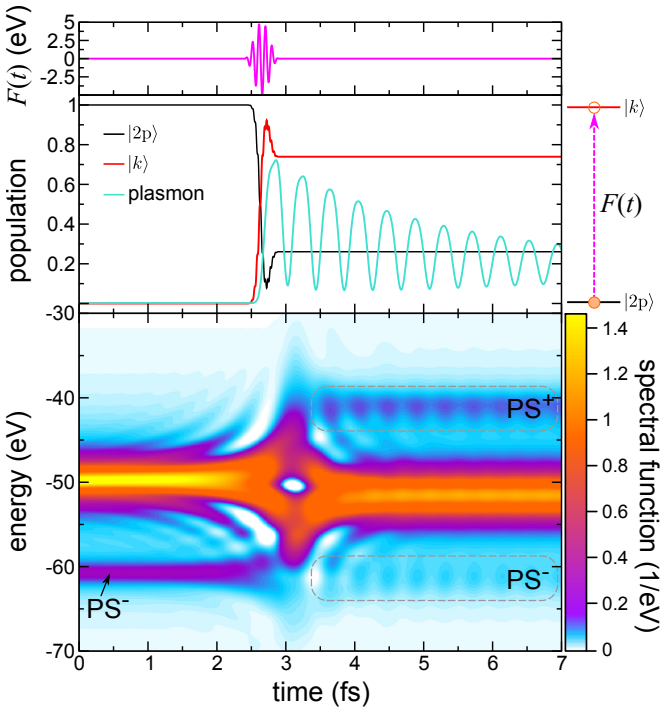

FIG. 5. Top panel: laser matrix element $F(t)$. Middle panel: population dynamics of the 2p and the photoelectron state along with the plasmon occupation. Bottom panel: time-dependent spectral function $A(T, \mathcal{E})$ of the core state. The Fourier transformation eq. (46) has been slightly smoothed by including exponential damping.

limit[19] of intrinsic plasmon excitation. The sudden change in the plasmon population is followed then by oscillations in the plasmon occupation. This nonequilibrium dynamics also becomes manifest in the time-resolved spectral function $A(T, \mathcal{E}) \equiv A_{2p,2p}(T, \mathcal{E})$ (fig. 5, bottom panel). The QP peak shifts transiently in about 1.5 fs from the initial configuration (QP peak at $\mathcal{E} = \mathcal{E}_{\mathrm{QP}}$, PS^- at $\mathcal{E}_{\mathrm{PS}^-} = 60.3$ eV[75] to the new QP position at $\mathcal{E} = -51.76$ eV. The shift is less than expected from equilibrium spectral function for the completely empty core state ($A^+(\mathcal{E})$, fig. 4(a)). The spectral density quenches transiently into the new equilibrium position. In this way the PS^- splits into a branch coalescing in the QP and a second one merging with the shifted PS^- after the pulse. A PS above the QP appears (PS^+) as expected. Furthermore, the strength of the $\mathrm{PS}^\pm$ oscillates in time. In order to understand this behavior one needs to take the bosonic occupation into account, as well. Revisiting the equilibrium case, fig. 4(c) depicts the spectral function of the occupied core state with fixed integer plasmon number $N_{\mathrm{pl}} = n$, $A^-_{(n)}(\mathcal{E})$. The presence of a plasmon gives rise to a PS on the right-hand side of the QP peak, describing plasmon-assisted photoemission (i. e., a plasmon can be absorbed, transferring its energy to the photoelectron). Increasing n leads to stronger boson fluctuations (cf. appendix B) and hence enhances the magnitude of the imaginary part of self-energy, leading to broadened spectral features. This is consistent with the broadening observed in fig. 4(c). Returning to the time-dependent scenario, these features are indeed manifested in $A(T, \mathcal{E})$ (fig. 5): the spectral strength of the $\mathrm{PS}^\pm$ displays oscillations in phase with the time-dependent plasmon occupation $N_{\mathrm{pl}}(t)$. Furthermore, the weight of the QP peak is suppressed anti-phase-wise to the variations of the PSs weight, as apparent from cuts of $A(T, \mathcal{E})$ at the characteristic energies (fig. 4(d)). Hence the spectral function exhibits an oscillatory transfer of spectral weight from the QP peak to the PSs. The enhanced broadening expected from fig. 4(c) is clearly visible in the spectral function at the end of the propagation $A(T_p, \mathcal{E})$, as compared to the equilibrium spectra $A^\pm(\mathcal{E})$ in fig. 4(a).

B. Time-resolved photoelectron spectra

After analyzing the intrinsic effects upon removing the electron from the core level, we proceed by incorporating extrinsic effects into the electron-plasmon coupling (43). Extrinsic plasmon losses are post-emission, or, in other words, scattering effects. This goes beyond the standard treatment of (time-resolved) photoemission in terms of the lesser GF restricted to bound states. Extrinsic effects can be incorporated by explicitly including (at least) two states $|k_1\rangle$, $|k_2\rangle$ representing photoelectrons and assign the plasmonic matrix element $\Gamma_{\mathrm{ex}} \equiv (\mathbf{\Gamma}_{\mathrm{ex}})_{k_1k_2} = (\mathbf{\Gamma}_{\mathrm{ex}})_{k_2k_1}$ (diagonal elements are set to zero). As photoelectrons propagate to infinity, the system is treated as open in their subspace. This is accomplished by including embedding self-energies. Because the continuum of photoelectron states describes electron propagating outside the sample, a non-interacting basis can be chosen. Defining the coupling density $U_{ij}(\mathcal{E}) = \sum_k V_{i,k} V^*_{k,j} \delta(\mathcal{E} - \epsilon_k)$, the continuum embedding self-energy can be expressed in spectral representation as

$$\mathbf{\Sigma}^{\mathrm{em},\gtrless}(t_1, t_2) = \int_0^\infty \frac{\mathrm{d}\mathcal{E}}{2\pi} \mathbf{\Sigma}^{\mathrm{em},\gtrless}(\mathcal{E}) e^{-\mathrm{i}\mathcal{E}(t_1 - t_2)} \,, \tag{47}$$

with

$$\mathbf{\Sigma}^{\mathrm{em},<}(\mathcal{E}) = \mathrm{i}\,\mathbf{U}(\mathcal{E}) N_F(\mathcal{E} - \mu) \,, \tag{48}$$

$$\mathbf{\Sigma}^{\mathrm{em},>}(\mathcal{E}) = -\mathrm{i}\,\mathbf{U}(\mathcal{E}) \left[1 - N_F(\mathcal{E} - \mu)\right] \,, \tag{49}$$

where $N_F(\mathcal{E})$ denotes the Fermi distribution function. $\mathbf{U}(\mathcal{E})$ accommodates the density of continuum states (e. g. proportional to $\sqrt{\mathcal{E}}$ for free particles) and matrix element effects. We simplify the expressions by approximating $\mathbf{U}(\mathcal{E}) \approx U_0 \mathbf{I}$ as a constant (WBLA). The retarded embedding self-energy attains $\mathbf{\Sigma}^{\mathrm{em,R}}(t_1, t_2) = -(\mathrm{i}/2) U_0 \delta(t_1 - t_2)$ in this case. In accordance with the physical picture we furthermore assume that no electrons can return from the continuum, leading to $\mathbf{\Sigma}^{\mathrm{em},<}(\mathcal{E}) \approx 0$. The WBLA has an advantage that all states, regardless of their energy, are damped uniformly. Such structureless embedding does not introduce any additional energy dependent time delays.

The embedding self-energy for continuum states furthermore allows for computing the photocurrent (the number of electrons emitted per unit of time) $J(\mathcal{E}, t) = \mathrm{d}n(\mathcal{E}, t)/\mathrm{d}t$ by the transient Meir-Wingreen formula[29,76] often used in transport calculations. The Meir-Wingreen expression for the total

electron current flowing out of system reads

$$\frac{\mathrm{d}n(t)}{\mathrm{d}t} = 4\mathrm{Re}\left\{\mathrm{Tr}_k[\mathbf{\Sigma}^{\mathrm{em,R}}\cdot\mathbf{G}^{<} + \mathbf{\Sigma}^{\mathrm{em},<}\cdot\mathbf{G}^{\mathrm{A}} + \mathbf{\Sigma}^{\mathrm{em},\ulcorner}\star\mathbf{G}^{\lceil}](t,t)\right\} . \tag{50}$$

Here, Tr_k stands for the partial trace over the photoelectron states $|k_{1,2}\rangle$. Eq. (50) is simplified in our case as $\mathbf{\Sigma}^{\mathrm{em},\ulcorner} = 0$ due to the adiabatic switching procedure and $\mathbf{\Sigma}^{\mathrm{em},<} = 0$ by the assumptions above. If we further resolve with respect to the photoelectron energies $\mathcal{E}$, we obtain

$$J(\mathcal{E},t) = 4U_0\,\mathrm{Im}\int_0^t \mathrm{d}\bar{t}\, e^{-\mathrm{i}\mathcal{E}(t-\bar{t})}\mathrm{Tr}_k\left[\mathbf{G}^{<}(\bar{t},t)\right] . \tag{51}$$

We solved the KBEs eq. (33) and (35) for the three-level system as in subsec. IV A (with the additional embedding self-energy included). In order to reflect the experimental situation[9] the photoelectron states are assigned energies $\mathcal{E}_{k_1} = 68$ eV and $\mathcal{E}_{k_2} = 58$ eV ($\mathcal{E}_{k_1} - \mathcal{E}_{k_2} = \Omega_{\mathrm{pl}}$). The laser frequency is chosen $\omega_{\mathrm{L}} = 118$ eV, corresponding to the transition $|2\mathrm{p}\rangle \rightarrow |k_1\rangle$. The pulse length is set to $\tau_{\mathrm{p}} = 1.2$ fs, corresponding to the full width at half-maximum of 450 attoseconds as in the experiment. The laser field amplitude is adjusted to perform a complete population transfer in a non-interacting reference system.

Both intrinsic and extrinsic losses can result in the population of $|k_2\rangle$ continuum state with a lower energy, which translates to a peak of $J(\mathcal{E},t)$ around $\mathcal{E} \sim 58$ eV (see illustration in fig. 6). The interplay between the two channels can be studied by turning either Γ_{in} or Γ_{ex} on or off (fig. 6). In case that electron-plasmon interaction is switched off completely, $|k_2\rangle$ acquires only a negligible occupation, while the transient photoelectron spectrum $J(\mathcal{E},t)$ converges to a dominant peak around $\mathcal{E} \sim 68$ eV (fig. 6(a)). The plasmon number N_{pl} stays, of course, constant. When including intrinsic losses (fig. 6(b)), $J(\mathcal{E},t)$ displays a peak originating from the emission from PS^-. Note that the $N_{\mathrm{pl}}(t)$ exhibits only small onset oscillations as compared to fig. 5 because of the slower ionization process due to the increased laser pulse duration. Pure extrinsic electron-plasmon interaction (fig. 6(c)) gives rise to similar spectral features, the occurrence of a peak in the time-resolved spectra is however delayed with respect to the intrinsic case. This is clear since $|k_2\rangle$ can only be populated as a result of additional scattering of $|k_1\rangle$ involving the creation of a plasmon. This transition rate is set by i) Γ_{ex}, ii) the plasmon frequency and iii) the population of $|k_1\rangle$. Turning to the case of comparable intrinsic and extrinsic losses (fig. 5(d)) the total number of photoelectrons detectable around $E \sim 56$ eV increases beyond the previous cases. Interestingly, the bump in the population of $|k_2\rangle$ due to extrinsic losses is less pronounced as in fig. 6(c) and delayed by ~ 120 as. On the other hand, the photocurrent extends over a longer period of time before approaching zero. Both factors are expected to influence the observed streaking time delay[9]. Moreover, the extrinsic process is weakened by the presence of intrinsic losses. This can be seen from that the maximum in the population of $|k_2\rangle$ is slightly less pronounced when comparing fig. 6(c) and (d). The intrinsic channel is already creating a plasmon, which acts as driving against extrinsic losses. This is a manifestation

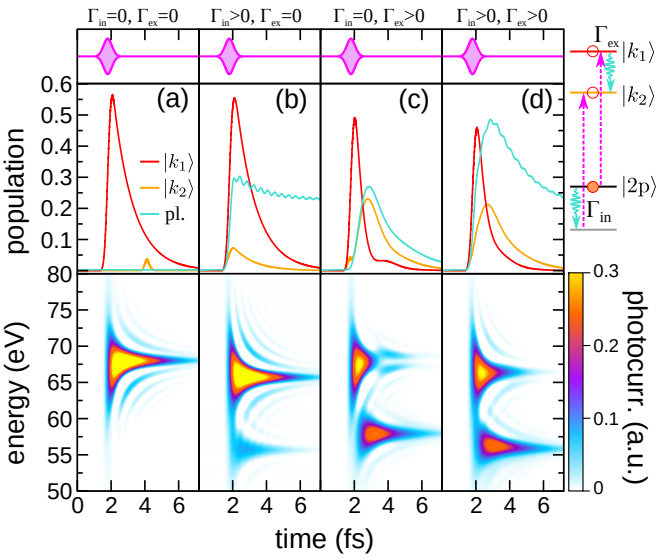

FIG. 6. Laser-induced KBE dynamics for the three-level system (see sketch on the right-hand side). Top panels: envelop of the laser pulse. Middle panels: population dynamics of $|k_{1,2}\rangle$ and the plasmon occupation. Bottom panels: time-resolved photocurrent $J(\mathcal{E},t)$. The electron-plasmon interaction is set to (a) $\Gamma_{\mathrm{in}} = \Gamma_{\mathrm{ex}} = 0$, (b) $\Gamma_{\mathrm{in}} = 5$ eV, $\Gamma_{\mathrm{ex}} = 0$, (c) $\Gamma_{\mathrm{in}} = 0$, $\Gamma_{\mathrm{ex}} = 1$ eV, and (d) $\Gamma_{\mathrm{in}} = 5$ eV, $\Gamma_{\mathrm{ex}} = 1$ eV. The magnitude of Γ_{ex} is chosen to put on a level with intrinsic/extrinsic effects.

of quantum interference between intrinsic and extrinsic losses, analogous to ref. 14. The plasmon dynamics is quite different in the intrinsic and extrinsic cases, as well. For intrinsic coupling only, the plasmon occupation quickly rises and is weakly damped due to the boson embedding self-energy. At variance, the plasmon creation is delayed in the extrinsic case and the plasmon occupation vanishes rapidly. The dynamics is governed here by a dynamical balance $|k_1\rangle \rightarrow |k_2\rangle$ upon creating plasmons and by the inverse process (visible in, e. g., the non-monotonic behavior of the population of the upper continuum state for $t > 2$ fs). As both continuum states are subject to environmental coupling, the transition $|k_2\rangle \rightarrow |k_1\rangle$ due to plasmon absorption leads to an effective plasmon damping.

V. CONCLUSIONS

In this work we developed a formalism for simultaneous propagation of the coupled fermionic and bosonic Kadanoff-Baym equations. The marked feature of our scheme is the treatment of bosonic correlators: coupled first-order equations of motions for $\langle\Delta\hat{Q}_\mu(z)\Delta\hat{Q}_\nu(z')\rangle$, $\langle\Delta\hat{Q}_\mu(z)\Delta\hat{P}_\nu(z')\rangle$, and $\langle\Delta\hat{P}_\mu(z)\Delta\hat{P}_\nu(z')\rangle$ correlators are reformulated as a second-order equation of motion for the coordinate-coordinate correlator and is efficiently propagated using the two-dimensional Numerov formula. The two-times nonequilibrium Green's functions, which are the solutions of these equations, completely describe the transient spectral density of both subsystems and allow to obtain the time-resolved photoemission

spectra. Several competing scattering mechanisms result in a photoelectron arriving at the detector with a lower energy and time delay as compared to the unscattered one. In our calculations of the photoemission from the 2p core state of bulk Mg we put apart scattering processes taking place before the photon interaction with the material and after the photoionization event on the electron's way to the detector. The time delay between the unscattered and scattered electrons is determined by the strength of electron-plasmon interaction which is the dominant scattering mechanism for electrons excited by the XUV photons as in the experiment[9]. Interference between these two scattering pathways has already been theoretically predicted to modify the spectral strength of plasmonic satellites. Here we demonstrate that the interference has also profound impact on the time dependence of the photoelectron current.

ACKNOWLEDGMENTS

This work is supported by the German Research Foundation (DFG) Collaborative Research Centre SFB 762 Functionality of Oxide Interfaces (J. B. and Y. P.) and Grant Number PA 1698/1-1 (M. S. and Y. P.).

Appendix A: Source-field method for deriving the equations of motion

Let us assume that our system is initially prepared in some canonical ensemble set by the inverse temperature β. Using contour-evolution operator, we can express the expectation value of any operator $\hat{O}$ by

$$\langle \hat{O}(z)\rangle = \frac{\mathrm{Tr}\left[\mathcal{T}\exp\left(-\mathrm{i}\int_C \mathrm{d}\bar{z}\hat{H}(\bar{z})\right)\hat{O}(z)\right]}{\mathrm{Tr}\left[\mathcal{T}\exp\left(-\mathrm{i}\int_C \mathrm{d}\bar{z}\hat{H}(\bar{z})\right)\right]} . \tag{A1}$$

Since embedding contributions to the self-energy are additive and straightforward to construct, we can focus on the electron-boson part, described by the general Hamiltonian

$$\hat{H}_0(z) = \sum_{ij} h_{ij}(z)\hat{c}_i^\dagger \hat{c}_j + \sum_\nu \sum_{ij} \Gamma^\nu_{ij}(z)\hat{c}_i^\dagger \hat{c}_j \hat{Q}_\nu + \sum_\nu \frac{\Omega_\nu(z)}{2}\left(\hat{P}_\nu^2 + \hat{Q}_\nu^2\right) . \tag{A2}$$

The Hamiltonian is now modified by adding time-dependent fields coupled to the bosons, that is

$$\hat{H}_\xi(z) = \hat{H}_0(z) + \sum_\nu \xi_\nu(z)\hat{Q}_\nu . \tag{A3}$$

The Heisenberg representation of all operators are now to be understood with respect to $\hat{H}_\xi(z)$. The way the source field couples to the system, the bosonic propagators can directly be obtained by

$$D_{\mu\nu}(z_1, z_2) = \left.\frac{\delta\langle \hat{Q}_\mu(z_1)\rangle}{\delta\xi_\nu(z_2)}\right|_{\xi_\nu=0} , \tag{A4}$$

showing again that the boson GF describes the fluctuation of the amplitude $\langle \hat{Q}_\nu(z_1)\rangle$. In the following, all functional derivatives with respect to $\xi_\nu(z)$ are understood to be taken at $\xi_\nu = 0$.

1. Fermionic Green's function and self-energy

With the help of the Heisenberg EOM, we obtain the fermion GF

$$\left(\mathrm{i}\frac{\partial}{\partial z_1} - \mathbf{h}(z_1)\right)\mathbf{G}(z_1, z_2) = \mathbf{I}\,\delta(z_1, z_2) + \sum_\nu \mathbf{\Gamma}^\nu(z_1)\,\mathbf{\Upsilon}^\nu(z_1, z_1^+, z_2) , \tag{A5}$$

with the higher-order correlator $\Upsilon^\nu_{kj}(z_1, z_2, z_3) = -\mathrm{i}\langle \mathcal{T}\hat{c}_k(z_1)\hat{Q}_\nu(z_2)c_j^\dagger(z_3)\rangle$. The superscript + denotes an infinitesimal shift to later times. It is straightforward to see that it can obtained by varying the fermionic GF with respect to the source field:

$$\mathbf{\Upsilon}^\nu(z_1, z_3, z_2) = \mathrm{i}\frac{\delta\mathbf{G}(z_1, z_2)}{\delta\xi_\nu(z_3)} + \langle \hat{Q}_\nu(z_3)\rangle\mathbf{G}(z_1, z_2) . \tag{A6}$$

Formally, we can identify the correlator term on the right-hand side of eq. (A5) with the self-energy term, i. e.

$$\sum_\nu \mathbf{\Gamma}^\nu(z_1)\mathbf{\Upsilon}^\nu(z_1, z_1^+, z_2) = \int_C \mathrm{d}z_3\, \mathbf{\Sigma}(z_1, z_3)\mathbf{G}(z_3, z_2) .$$

In order to access the self-energy directly, we need the inverse GF. In particular, let us define the right-inverse by

$$\int_C \mathrm{d}z_3\, \mathbf{G}(z_1, z_3)\overleftarrow{\mathbf{G}}^{-1}(z_3, z_2) = \mathbf{I}\,\delta(z_1, z_2) . \tag{A7}$$

Multiplying by $\overleftarrow{\mathbf{G}}^{-1}(z_3, z_2)$ and integrating over z_3 yields for the self-energy

$$\mathbf{\Sigma}(z_1, z_2) = \sum_\nu \mathbf{\Gamma}^\nu(z_1)\int_C \mathrm{d}(z_3 z_4)\,\mathbf{\Upsilon}^\nu(z_1, z_4, z_3)\overleftarrow{\mathbf{G}}^{-1}(z_3, z_2)\delta(z_1^+, z_4) .$$

Eq. (A6) suggests a separation of the self-energy into two terms. For reasons that will become clear below, this distinction amounts to splitting the self-energy into a mean-field and correlation (c) part. The mean-field part gives

$$\mathbf{\Sigma}^{\mathrm{MF}}(z_1, z_2) = \delta(z_1, z_2)\sum_\nu \mathbf{\Gamma}^\nu(z_1)\langle \hat{Q}_\nu(z_1)\rangle .$$

The correlation part of the self-energy so far reads

$$\mathbf{\Sigma}^{\mathrm{c}}(z_1, z_2) = \mathrm{i}\sum_\nu \mathbf{\Gamma}^\nu \int_C \mathrm{d}(z_3 z_4)\frac{\delta\mathbf{G}(z_1, z_3)}{\delta\xi_\nu(z_4)}\overleftarrow{\mathbf{G}}^{-1}_{nj}(z_3, z_2)\delta(z_1^+, z_4) .$$

Let us introduce the new source field

$$\zeta_{ab}(z) = \sum_\nu \Gamma^\nu_{ab}(z)\langle \hat{Q}_\nu(z)\rangle , \tag{A8}$$

which is exactly the mean-field contribution to the fermionic self-energy. This is analogous to the case of Hedin's equations, where the original source field (coupling to the density)

is replaced by the total electronic energy. The reasons for the modification is to carry out the variation of the fermionic GF with respect to fermionic quantities only. Using the chain rule for functional derivatives, we obtain

$$\Sigma^{\mathrm{c}}_{ij}(z_1,z_2) = \mathrm{i}\sum_{\nu}\sum_{nk}\sum_{ab}\Gamma^{\nu}_{ik}(z_1)\int_C \mathrm{d}(z_3z_4z_5)\frac{\delta G_{kn}(z_1,z_3)}{\delta\zeta_{ab}(z_5)} \times \overleftarrow{G}^{-1}_{nj}(z_3,z_2)\frac{\delta\zeta_{ab}(z_5)}{\delta\xi_{\nu}(z_4)}\delta(z_1^+,z_4)\,.$$

Invoking the functional variation analog of integration by parts, we can transfer the variation with respect to $\zeta_{ab}(z_5)$ to the inverse GF. Noting further $\delta\zeta_{ab}(z_5)/\delta\xi_{\nu}(z_4) = \Gamma^{\mu}_{ab}(z_5)D_{\mu\nu}(z_5,z_4)$ one arrives at

$$\Sigma^{\mathrm{c}}_{ij}(z_1,z_2) = \mathrm{i}\sum_{\mu\nu}\sum_{nk}\sum_{ab}\int_C \mathrm{d}(z_3z_5)\Gamma^{\mu}_{ab}(z_5)G_{kn}(z_1,z_3) \times \Lambda_{njab}(z_3,z_2;z_5)D_{\mu\nu}(z_5,z_1^+)\Gamma^{\nu}_{ik}(z_1)\,,$$

where we have introduced the three-point vertex

$$\Lambda_{abcd}(z_1,z_2;z_3) = -\frac{\delta\overleftarrow{G}^{-1}_{ab}(z_1,z_2)}{\delta\zeta_{cd}(z_3)}\,. \tag{A9}$$

2. Vertex function and Bethe-Salpeter equation

The definition of the vertex function eq. (A9) is completely analogous to the derivation of Hedin's equations by the source-field method. Beside this correspondence, treating the object $\Lambda_{abcd}(z_1,z_2;z_3)$ as the usual vertex function is justified as it obeys the Bethe-Salpeter equation (BSE). In order to show this property, we first realize that

$$\overleftarrow{G}^{-1}_{ab}(z_1,z_2) = \left(-\mathrm{i}\frac{\overleftarrow{\partial}}{\partial z_1}\delta_{ab} - \zeta_{ab}(z_1)\right)\delta(z_1,z_2) - \epsilon_a\delta_{ab} - \Sigma^{\mathrm{c}}_{ab}(z_1,z_2)$$

and thus

$$\Lambda_{abcd}(z_1,z_2;z_3) = \delta_{ac}\delta_{bd}\delta(z_1,z_2)\delta(z_1,z_3) + \frac{\delta\Sigma^{\mathrm{c}}_{ab}(z_1,z_2)}{\delta\zeta_{cd}(z_3)}\,. \tag{A10}$$

Similar to the strategy above, we employ the chain rule for functional variation for the second term in eq. (A10) to transform

$$\frac{\delta\Sigma^{\mathrm{c}}_{ab}(z_1,z_2)}{\delta\zeta_{cd}(z_3)} = \sum_{mn}\int_C \mathrm{d}(z_4z_5)\frac{\delta\Sigma^{\mathrm{c}}_{ab}(z_1,z_2)}{\delta G_{mn}(z_4,z_5)}\frac{\delta G_{mn}(z_4,z_5)}{\delta\zeta_{cd}(z_3)}\,.$$

As usual, we introduce the four-point kernel for BSE as

$$K_{abcd}(z_1,z_2;z_3,z_4) = \frac{\delta\Sigma^{\mathrm{c}}_{ab}(z_1,z_2)}{\delta G_{cd}(z_3,z_4)}\,. \tag{A11}$$

Next, we would like to express the variation $\delta G_{mn}(z_4,z_5)/\delta\zeta_{cd}(z_3)$ by the inverse GF in order to close the equation. This can be achieved by inserting the unity relation eq. (A7). We thus obtain

$$\begin{aligned}\frac{\delta\Sigma^{\mathrm{c}}_{ab}(z_1,z_2)}{\delta\zeta_{cd}(z_3)} &= \sum_{mn}\sum_{p}\int_C \mathrm{d}(z_4z_5z_6)K_{abmn}(z_1,z_2;z_4,z_5) \times \frac{\delta G_{mp}(z_4,z_6)}{\delta\zeta_{cd}(z_3)}\delta_{pn}\delta(z_5,z_6)\\ &= \sum_{mn}\sum_{pq}\int_C \mathrm{d}(z_4z_5z_6z_7)K_{abmn}(z_1,z_2;z_4,z_5) \times \frac{\delta G_{mp}(z_4,z_6)}{\delta\zeta_{cd}(z_3)}G_{pq}(z_5,z_7)\overleftarrow{G}^{-1}_{qn}(z_7,z_6)\,.\end{aligned}$$

Now we apply the variation to $\overleftarrow{G}^{-1}_{qn}(z_7,z_6)$, which then amounts to $\Lambda_{qncd}(z_7,z_6;z_3)$. Finally, we obtain the BSE

$$\begin{aligned}\Lambda_{abcd}(z_1,z_2;z_3) &= \delta_{ac}\delta_{bd}\delta(z_1,z_2)\delta(z_1,z_3) + \sum_{mn}\sum_{pq}\int_C \mathrm{d}(z_4z_5z_6z_7)K_{abmn}(z_1,z_2;z_4,z_5) \times G_{mp}(z_4,z_6)G_{pq}(z_5,z_7)\Lambda_{qncd}(z_7,z_6;z_3)\,.\end{aligned} \tag{A12}$$

3. Boson Green's function and polarization

By differentiating the position-position correlator twice using EOM for position (18) and momentum (19) operators we arrive at the second order differential equation

$$-\frac{1}{\Omega_{\mu}(z_1)}\left(\frac{\partial^2}{\partial z_1^2} + \Omega^2_{\mu}(z_1)\right)D_{\mu\nu}(z_1,z_2) = \delta_{\mu\nu}\delta(z_1,z_2) + \mathrm{Tr}\left[\mathbf{\Gamma}^{\mu}(z_1)\frac{\mathrm{i}\,\delta\mathbf{G}(z_1,z_1^+)}{\delta\xi_{\nu}(z_2)}\right]\,.$$

Here, we omit the terms originating from the bath bosonic coordinates. They can be added straightforwardly. In order to close the EOM we introduce the irreducible polarization

$$P_{abcd}(z_1,z_2) = -\mathrm{i}\frac{\delta G_{ab}(z_1,z_1^+)}{\delta\zeta_{cd}(z_2)}\,. \tag{A13}$$

Like for the fermion GF we introduce the (right) inverse boson GF according to

$$\sum_{\xi}\int_C \mathrm{d}z_3\, D_{\mu\xi}(z_1,z_3)[\overleftarrow{D}^{-1}]_{\xi\nu}(z_3,z_2) = \delta_{\mu\nu}\delta(z_1,z_2)\,. \tag{A14}$$

Hence, we can express the polarization part of self-energy $\Pi^{\mathrm{p}}_{\mu\nu}(z_1,z_2)$ for the bosons, implicitly defined by

$$\mathrm{Tr}\left[\mathbf{\Gamma}^{\mu}(z_1)\,\mathrm{i}\frac{\delta\mathbf{G}(z_1,z_1^+)}{\delta\xi_{\nu}(z_2)}\right] = \sum_{\zeta}\int_C \mathrm{d}z_3\,\Pi^{\mathrm{p}}_{\mu\zeta}(z_1,z_3)D_{\zeta\nu}(z_3,z_2)\,, \tag{A15}$$

as

$$\begin{aligned}\Pi^{\mathrm{p}}_{\mu\nu}(z_1,z_2) &= \mathrm{Tr}\left[\mathbf{\Gamma}^{\mu}(z_1)\int_C \mathrm{d}z_3 \frac{\mathrm{i}\delta\mathbf{G}(z_1,z_1^+)}{\delta\xi_\zeta(z_3)}[\overleftarrow{D}^{-1}]_{\zeta\nu}(z_3,z_2)\right]\\ &= \sum_{mn}\sum_{ij}\Gamma^{\mu}_{ij}(z_1)\int_C \mathrm{d}(z_3z_4)\frac{\mathrm{i}\delta G_{ji}(z_1,z_1^+)}{\delta\zeta_{mn}(z_4)}\frac{\delta\zeta_{mn}(z_4)}{\delta\xi_\zeta(z_3)}\\ &\quad\times[\overleftarrow{D}^{-1}]_{\zeta\nu}(z_3,z_2)\end{aligned}$$

and thus

$$\Pi^{\mathrm{p}}_{\mu\nu}(z_1,z_2) = \sum_{mn}\sum_{ij}\Gamma^{\mu}_{ij}(z_1)\Gamma^{\nu}_{mn}(z_2)P_{jimn}(z_1,z_2)\,. \tag{A16}$$

Finally, we investigate how the polarization $P_{abcd}(z_1,z_2)$ can be correlated to the fermionic GF. For this purpose we invoke the rule

$$\begin{aligned}\frac{\delta G_{ab}(z_1,z_2)}{\delta\zeta_{cd}(z_5)} &= -\sum_{pq}\int_C \mathrm{d}(z_3z_4)G_{ap}(z_1,z_3)\frac{\delta\overleftarrow{G}^{-1}_{pq}(z_3,z_4)}{\delta\zeta_{cd}(z_5)}\\ &\quad\times G_{qb}(z_4,z_2)\,,\end{aligned} \tag{A17}$$

from which we obtain

$$\begin{aligned}P_{abcd}(z_1,z_2) &= -\mathrm{i}\sum_{pq}\int_C \mathrm{d}(z_3z_4)G_{ap}(z_1,z_3)G_{qb}(z_4,z_1^+)\\ &\quad\times\Lambda_{pqcd}(z_3,z_4;z_2)\,.\end{aligned} \tag{A18}$$

Appendix B: Basic properties of the boson propagator

From the definition eq. (13) one infers $D_{\mu\nu}(z_1,z_2) = D_{\nu\mu}(z_2,z_1)$. This implies for the greater/lesser Keldysh components

$$D^{\gtrless}_{\mu\nu}(t_1,t_2) = D^{\lessgtr}_{\nu\mu}(t_2,t_1)\,, \tag{B1}$$

such that the retarded boson propagator becomes a real function:

$$\begin{aligned}D^{\mathrm{R}}_{\mu\nu}(t_1,t_2) &= \theta(t_1-t_2)\left[D^{>}_{\mu\nu}(t_1,t_2)-D^{<}_{\mu\nu}(t_1,t_2)\right]\\ &= 2\theta(t_1-t_2)\mathrm{Re}\left[D^{>}_{\mu\nu}(t_1,t_2)\right]\,.\end{aligned} \tag{B2}$$

Similarly, one obtains $D^{\mathrm{A}}_{\mu\nu}(t_1,t_2) = (D^{\mathrm{R}}_{\nu\mu}(t_2,t_1))^* = D^{\mathrm{R}}_{\nu\mu}(t_2,t_1)$ for the advanced GF. For the Matsubara component on the other hand, $D^{\mathrm{M}}_{\mu\nu}(\tau_1-\tau_2) = D_{\mu\nu}(t_0-\mathrm{i}\tau_1,t_0-\mathrm{i}\tau_2)$, the symmetry

$$D^{\mathrm{M}}_{\mu\nu}(\tau) = D^{\mathrm{M}}_{\nu\mu}(-\tau) \tag{B3}$$

holds. Hence, as compared to fermions or bosons with a single peak in a spectral function representing one QP, there is no discontinuity in the diagonal Matsubara function for the transition $\tau = 0^-$ to $\tau = 0^+$.

In equilibrium one can, as usual, assume that the greater/lesser propagators (and thus the retarded and advanced, as well) depend on the time difference $t_1 - t_2$ only. Therefore we can switch to frequency space $D^{\gtrless}_{\nu}(\omega) = \int \mathrm{d}t\, e^{\mathrm{i}\omega t}D^{\gtrless}_{\nu}(t)$. The symmetry relation eq. (B1) implies

$$D^{\gtrless}_{\mu\nu}(\omega) = D^{\lessgtr}_{\nu\mu}(-\omega)\,. \tag{B4}$$

The spectral function is obtained from

$$B_{\mu\nu}(\omega) = \mathrm{i}\left[D^{>}_{\mu\nu}(\omega) - D^{<}_{\mu\nu}(\omega)\right]\,, \tag{B5}$$

which, in turn, allows to characterize the greater/lesser boson GF by the fluctuation-dissipation theorem

$$D^{<}_{\mu\nu}(\omega) = -\mathrm{i}N_{\mathrm{B}}(\omega)B_{\mu\nu}(\omega)\,, \tag{B6a}$$

$$D^{>}_{\mu\nu}(\omega) = -\mathrm{i}(N_{\mathrm{B}}(\omega)+1)B_{\mu\nu}(\omega)\,, \tag{B6b}$$

where $N_{\mathrm{B}}(\omega)$ is the Bose distribution function. For illustration, let us consider the non-interaction case. From the definition eq. (13) the bare boson GF follows as

$$\begin{aligned}d^{\gtrless}_{\nu}(t_1,t_2) &= -\frac{\mathrm{i}}{2}\left[(N_\nu+1)e^{\mp\mathrm{i}\Omega_\nu(t_1-t_2)}+N_\nu e^{\pm\mathrm{i}\Omega_\nu(t_1-t_2)}\right]\\ &= \mp\frac{1}{2}\sin\left[\Omega_\nu(t_1-t_2)\right]-\mathrm{i}\left(N_\nu+\frac{1}{2}\right)\cos\left[\Omega_\nu(t_1-t_2)\right]\end{aligned} \tag{B7}$$

(in thermal equilibrium $N_\nu = N_{\mathrm{B}}(\Omega_\nu)$) and

$$d^{\mathrm{R}}_{\nu}(t_1,t_2) = -\theta(t_1-t_2)\sin\left[\Omega_\nu(t_1-t_2)\right]\,. \tag{B8}$$

Fourier transforming Eq. (B7) yields

$$d^{\gtrless}_{\nu}(\omega) = -\mathrm{i}\pi\left[(N_\nu+1)\delta(\omega\mp\Omega_\nu)+N_\nu\delta(\omega\pm\Omega_\nu)\right]\,, \tag{B9}$$

from which the spectral function follows as

$$b_{\mu\nu}(\omega) = \pi\delta_{\mu\nu}\Big(\delta(\omega-\Omega_\nu)-\delta(\omega+\Omega_\nu)\Big)\,. \tag{B10}$$

Using the property $N_{\mathrm{B}}(-\omega) = -(N_{\mathrm{B}}(\omega)+1)$ the normalization of the spectral function can be verified:

$$\int_{-\infty}^{\infty}\frac{\mathrm{d}\omega}{2\pi}N_{\mathrm{B}}(\omega)b_{\mu\nu}(\omega) = \delta_{\mu\nu}N_{\mathrm{B}}(\Omega_\nu)+\frac{1}{2}\,. \tag{B11}$$

The retarded GF reads

$$d^{\mathrm{R}}_{\nu}(\omega) = \frac{\Omega_\nu}{(\omega+\mathrm{i}\eta)^2-\Omega_\nu^2}\,, \tag{B12}$$

where η is a positive infinitesimal. By complex continuation one finds, analogously to eq. (B7), the non-interacting boson Matsubara function as

$$\begin{aligned}d^{\mathrm{M}}_{\nu}(\tau) &= -\frac{\mathrm{i}}{2}\left[(N_\nu+1)e^{-\Omega_\nu|\tau|}+N_\nu e^{\Omega_\nu|\tau|}\right]\\ &= \frac{\mathrm{i}}{2}\sinh(\Omega_\nu|\tau|)-\mathrm{i}\left(N_\nu+\frac{1}{2}\right)\cosh(\Omega_\nu\tau)\,.\end{aligned} \tag{B13}$$

Appendix C: Two-dimensional Numerov formula

Consider the differential equation

$$\left(\frac{\partial^2}{\partial t_1^2}+\frac{\partial^2}{\partial t_2^2}\right)F(t_1,t_2)+S(t_1,t_2) = 0\,, \tag{C1}$$

which we would like to solve numerically on a uniform two-dimensional mesh up to fourth order in the grid spacing Δt. This can be achieved by applying the Numerov discretization method, which can be summarized in a compact way by

$$\sum_{i=-1}^{1}\sum_{j=-1}^{1}\Big[(\Delta t)^2(A_iB_j + A_jB_i)F(t_1 + i\Delta t, t_2 + j\Delta t) + (\Delta t)^4 B_iB_jS(t_1 + i\Delta t, t_2 + j\Delta t)\Big] = 0\,. \tag{C2}$$

The coefficients are defined by

$$A_{-1} = 12\,, \quad A_0 = -24\,, \quad A_1 = 12\,, \tag{C3a}$$

$$B_{-1} = 1\,, \quad B_0 = 10\,, \quad B_1 = 1\,. \tag{C3b}$$

Solving eq. (C2), for instance, for $F(t_1 + \Delta t, t_2 + \Delta t)$ yields a fourth-order forward recursion formula.

* michael.schueler@physik.uni-halle.de

1 M. Kling and M. Vrakking, Annu. Rev. Phys. Chem. **59**, 463 (2008).
2 F. Krausz and M. Ivanov, Rev. Mod. Phys. **81**, 163 (2009).
3 S. Nagele, R. Pazourek, J. Feist, K. Doblhoff-Dier, C. Lemell, K. Tőkési, and J. Burgdörfer, J. Phys. B **44**, 081001 (2011).
4 R. Pazourek, S. Nagele, and J. Burgdörfer, Faraday Discussions **163**, 353 (2013).
5 E. Goulielmakis, Z.-H. Loh, A. Wirth, R. Santra, N. Rohringer, V. S. Yakovlev, S. Zherebtsov, T. Pfeifer, A. M. Azzeer, M. F. Kling, S. R. Leone, and F. Krausz, Nature **466**, 739 (2010).
6 F. Lépine, G. Sansone, and M. J. J. Vrakking, Chem. Phys. Lett. **578**, 1 (2013).
7 A. L. Cavalieri, N. Müller, T. Uphues, V. S. Yakovlev, A. Baltuška, B. Horvath, B. Schmidt, L. Blümel, R. Holzwarth, S. Hendel, M. Drescher, U. Kleineberg, P. M. Echenique, R. Kienberger, F. Krausz, and U. Heinzmann, Nature **449**, 1029 (2007).
8 S. Neppl, R. Ernstorfer, A. L. Cavalieri, C. Lemell, G. Wachter, E. Magerl, E. M. Bothschafter, M. Jobst, M. Hofstetter, U. Kleineberg, J. V. Barth, D. Menzel, J. Burgdörfer, P. Feulner, F. Krausz, and R. Kienberger, Nature **517**, 342 (2015).
9 C. Lemell, S. Neppl, G. Wachter, K. Tőkési, R. Ernstorfer, P. Feulner, R. Kienberger, and J. Burgdörfer, Phys. Rev. B **91**, 241101 (2015).
10 M. Lucchini, L. Castiglioni, L. Kasmi, P. Kliuiev, A. Ludwig, M. Greif, J. Osterwalder, M. Hengsberger, L. Gallmann, and U. Keller, Phys. Rev. Lett. **115**, 137401 (2015).
11 S. Hüfner, *Photoelectron Spectroscopy: Principles and Applications* (Springer Science & Business Media, 2003).
12 C. N. Berglund and W. E. Spicer, Phys. Rev. **136**, A1030 (1964).
13 D. C. Langreth, Phys. Rev. B **1**, 471 (1970).
14 L. Campbell, L. Hedin, J. J. Rehr, and W. Bardyszewski, Phys. Rev. B **65**, 064107 (2002).
15 M. Guzzo, G. Lani, F. Sottile, P. Romaniello, M. Gatti, J. J. Kas, J. J. Rehr, M. G. Silly, F. Sirotti, and L. Reining, Phys. Rev. Lett. **107**, 166401 (2011).
16 E. Klevak, J. J. Kas, and J. J. Rehr, Phys. Rev. B **89** (2014).
17 J. Lischner, D. Vigil-Fowler, and S. G. Louie, Phys. Rev. Lett. **110**, 146801 (2013).
18 Y. Pavlyukh, M. Schüler, and J. Berakdar, Phys. Rev. B **91**, 155116 (2015).
19 L. Hedin, J. Michiels, and J. Inglesfield, Phys. Rev. B **58**, 15565 (1998).
20 B. I. Lundqvist, Phys. Kondens. Mater. **9**, 236 (1969).
21 P. Minnhagen, J. Phys. C **8**, 1535 (1975).
22 F. Aryasetiawan and O. Gunnarsson, Rep. Prog. Phys. **61**, 237 (1998).
23 M. Cini and A. D'Andrea, J. Phys. C **21**, 193 (1988).
24 P. Lipavsky, V. Spicka, and B. Velicky, Phys. Rev. B **34**, 6933 (1986).
25 J. Freericks, H. Krishnamurthy, and T. Pruschke, Phys. Rev. Lett. **102** (2009).
26 C. Sohrt, A. Stange, M. Bauer, and K. Rossnagel, Faraday Discuss. **171**, 243 (2014).
27 S. Wall, D. Wegkamp, L. Foglia, K. Appavoo, J. Nag, R. F. H. Jr, J. Stähler, and M. Wolf, Nature Communications **3**, 721 (2012).
28 N. E. Dahlen and R. van Leeuwen, Phys. Rev. Lett. **98**, 153004 (2007).
29 P. Myöhänen, A. Stan, G. Stefanucci, and R. van Leeuwen, Phys. Rev. B **80**, 115107 (2009).
30 K. Balzer and M. Bonitz, *Nonequilibrium Green's Functions Approach to Inhomogeneous Systems* (Springer, 2012).
31 M. P. von Friesen, C. Verdozzi, and C.-O. Almbladh, Phys. Rev. Lett. **103** (2009).
32 M. Puig von Friesen, C. Verdozzi, and C.-O. Almbladh, Phys. Rev. B **82**, 155108 (2010).
33 C. Verdozzi, D. Karlsson, M. Puig von Friesen, C. O. Almbladh, and U. von Barth, Chem. Phys. Open problems and new solutions in time dependent density functional theory, **391**, 37 (2011).
34 A. J. White and M. Galperin, Phys. Chem. Chem. Phys. **14**, 13809 (2012).
35 G. D. Mahan, *Many-Particle Physics* (Springer Science & Business Media, 2000).
36 M. Galperin, M. A. Ratner, and A. Nitzan, Nano Lett. **4**, 1605 (2004).
37 L. K. Dash, H. Ness, and R. W. Godby, J. Chem. Phys. **132**, 104113 (2010).
38 M. Sukharev and M. Galperin, Phys. Rev. B **81** (2010).
39 H. Ness and L. K. Dash, Phys. Rev. B **84**, 235428 (2011).
40 M. Schüler, Y. Pavlyukh, and J. Berakdar, J. Phys. Chem. Lett. **4**, 1131 (2013).
41 E. Boström, A. Mikkelsen, and C. Verdozzi, arXiv:1507.06975 [cond-mat, physics:physics] (2015).
42 C. Pellegrini, J. Flick, I. V. Tokatly, H. Appel, and A. Rubio, Phys. Rev. Lett. **115**, 093001 (2015).
43 A. J. White, B. D. Fainberg, and M. Galperin, J. Phys. Chem. Lett. **3**, 2738 (2012).
44 K. Kaasbjerg and A. Nitzan, Phys. Rev. Lett. **114**, 126803 (2015).
45 M. Sentef, A. F. Kemper, B. Moritz, J. K. Freericks, Z.-X. Shen, and T. P. Devereaux, Physical Review X **3**, 041033 (2013).

[46] M. Eckstein and P. Werner, Phys. Rev. Lett. **110**, 126401 (2013).
[47] M. Guzzo, J. J. Kas, L. Sponza, C. Giorgetti, F. Sottile, D. Pierucci, M. G. Silly, F. Sirotti, J. J. Rehr, and L. Reining, Phys. Rev. B **89**, 085425 (2014).
[48] J. Vinson, J. J. Rehr, J. J. Kas, and E. L. Shirley, Phys. Rev. B **83**, 115106 (2011).
[49] J. J. Kas, F. D. Vila, J. J. Rehr, and S. A. Chambers, Phys. Rev. B **91**, 121112 (2015).
[50] J. J. Kas, A. P. Sorini, M. P. Prange, L. W. Cambell, J. A. Soininen, and J. J. Rehr, Phys. Rev. B **76**, 195116 (2007).
[51] C. O. Almbladh and P. Minnhagen, Phys. Rev. B **17**, 929 (1978).
[52] C.-O. Almbladh, Phys. Rev. B **34**, 3798 (1986).
[53] J. E. Inglesfield, J. Phys. C **16**, 403 (1983).
[54] D. R. Penn, Phys. Rev. Lett. **40**, 568 (1978).
[55] D. R. Penn, Phys. Rev. Lett. **38**, 1429 (1977).
[56] C.-O. Almbladh, Phys. Scr. **32**, 341 (1985).
[57] T. Fujikawa, J. Electron. Spectrosc. Relat. Phenom. **173**, 51 (2009).
[58] J.-J. Chang and D. C. Langreth, Phys. Rev. B **8**, 4638 (1973).
[59] T. Fujikawa and H. Arai, J. Electron. Spectrosc. Relat. Phenom. **123**, 19 (2002).
[60] L. Hedin and J. D. Lee, Phys. Rev. B **64**, 115109 (2001).
[61] A.-M. Uimonen, G. Stefanucci, and R. v. Leeuwen, J. Chem. Phys. **140**, 18A526 (2014).
[62] G. Pal, Y. Pavlyukh, H. C. Schneider, and W. Hübner, Eur. Phys. J. B **70**, 483 (2009).
[63] G. Pal, Y. Pavlyukh, W. Hübner, and H. C. Schneider, Eur. Phys. J. B **79**, 327 (2011).
[64] A. S. Moskalenko, Y. Pavlyukh, and J. Berakdar, Phys. Rev. A **86**, 013202 (2012).
[65] E. Perfetto, D. Sangalli, A. Marini, and G. Stefanucci, arXiv:1507.01786 [cond-mat] (2015).
[66] G. Stefanucci and R. v. Leeuwen, *Nonequilibrium Many-Body Theory of Quantum Systems: A Modern Introduction* (Cambridge University Press, 2013).
[67] G. Strinati, Riv. Nuovo Cimento **11**, 1 (1988).
[68] G. Baym and L. P. Kadanoff, Phys. Rev. **124**, 287 (1961).
[69] L. P. Kadanoff and G. Baym, *Quantum Statistical Mechanics* (Addison-Wesley, 1994).
[70] J. Viljas, J. Cuevas, F. Pauly, and M. Häfner, Phys. Rev. B **72** (2005).
[71] N. Säkkinen, Y. Peng, H. Appel, and R. van Leeuwen, arXiv:1507.04726 [cond-mat] (2015).
[72] A. Stan, N. E. Dahlen, and R. v. Leeuwen, J. Chem. Phys. **130**, 224101 (2009).
[73] The factor $1/2$ when comparing to ref. 13 is due to the different definition of the electron-boson coupling (4).
[74] U. Weiss, *Quantum Dissipative Systems* (World Scientific, 2012).
[75] Note the distance between QP peaks and PSs is overestimated by the *GW* approximation and slightly modified by the finite width of the boson spectral function due to embedding.
[76] A.-P. Jauho, N. S. Wingreen, and Y. Meir, Phys. Rev. B **50**, 5528 (1994).